Journal of Superconductivity and Novel Magnetism (2022) 35:3565–3571
https://doi.org/10.1007/s10948-022-06383-6

Effects of Ion-Doping at A Site and B Site on Structure and Magnetic Properties of $BiFeO_3$ Nanoparticles

Yan Wang[1]

Received: 1 June 2022 / Accepted: 17 August 2022 / Published online: 25 August 2022

Abstract
Multiferroic $BiFeO_3$ and 10% La/Mn-doped $BiFeO_3$ powder samples were synthesized by conventional hydrothermal method to study the substitution at different sites driven by structural transformation and magnetic property in $BiFeO_3$. Room-temperature X-ray diffraction (XRD) patterns identified the rhombohedral *R*3*c* symmetry for all samples and further confirmed by the Bi-L_3 edge and Fe-*K* edge X-ray absorption fine structure (XAFS) spectra. However, a nanoscale phase transition from *R*3*c* structure to orthorhombic symmetry was revealed by the La-L_3 edge XAFS. In contrast, the Mn-doped $BiFeO_3$ remained *R*3*c* crystal structure. Besides, the variation of magnetism due to A-site and B-site substitution in $BiFeO_3$ was observed in the magnetic hysteresis loops.

Keywords Multiferroic materials · XAFS · Substitution · Structural phase transition

1 Introduction

Multiferroic materials exhibiting coexistence of ferroelectric (or antiferroelectric) and ferromagnetic (or antiferromagnetic) ordering have attracted much attention due to their fascinating fundamental physics as well as the potential applications in multistate memories, information storage, and spintronics devices [1–3]. Among the prototypical multiferroic oxide with the perovskite structure (ABO_3), $BiFeO_3$ (BFO) has been intensively studied because of its relatively high antiferromagnetic Neel temperature ($T_N \sim 640$ K) and ferroelectric Curie temperature ($T_C \sim 1100$ K), which make it possible for potential applications as optical and magnetic materials at room temperature [4–6].

Although BFO presents outstanding advantages, its practical applications were hampered by several crucial problems, such as the low resistivity and large loss factor arising out of oxygen non-stoichiometry, the leakage current problems because of impurities, and the cancellation of the ion magnetic moments in the bulk materials due to the canted G-type antiferromagnetic order by its spatial periodic inhomogeneous spin structure [7–9]. To overcome these problems, a number of considerable efforts have been made. Among the various ways, lattice site substitutions in BFO with different chemical composition has been confirmed to be an effective and economical method to improve the multiferroic properties of BFO according to lots of researches [3, 5, 6, 10, 11], such as A-site substitution with rare earth ions (Gd, Dy, and Sm etc.) [12, 13] and B-site substitution with alkaline earth ions (Cr, Ca, and Ba etc.) [9, 14, 15] in the perovskite-like $BiFeO_3$ (ABO_3, A = Bi and B = Fe). Among the various doping elements, the ionic radius of La^{3+} is similar to that of Bi^{3+}, and the ionic radius of Mn^{3+} is closer to that of Fe^{3+}; therefore, La and Mn ions were usually chosen for doping at Bi and Fe site, respectively, and many studies have carried out around these two doping situations. For the obvious changes in multiferroic performance in La/Mn-substituted BFO samples, the doping-induced phase transitions were considered to be the main reason [16–20]. However, more studies have found that there are also changes in the physical properties of doped BFO without phase transition, and especially the magnetic behaviors, which are believed to originate from partially filled 3*d* orbital of Fe and inhibited by the cycloid spin structure with the periodicity of 62 nm, are more vulnerable to the substitution [21]. As a result, few conclusions are proposed, such as the undesired second phase, the distortion of the local structure, the changing of the Fe–O–Fe angle, the DM interaction by disturbing the Fe–O bond, and the suppressing of the peculiar spiral spin structure [22–25], which are widely accepted in La/Mn-substituted BFO samples [26–28], but apparently the

✉ Yan Wang
wy@cidp.edu.cn

[1] Institute of Disaster Prevention, Hebei 065201, China

explanations are full of controversy, and the reasons of performance changes have been a long-standing problem to be explored. In addition, accurate information about the local structure of doped samples is extremely important, especially secondary nanosized particles with orthorhombic symmetry structure were discovered in $Bi_{0.95}La_{0.05}FeO_3$ [29]; hence, the structure-sensitive tools are desperately needed to strictly identify the local structure around doped elements and further understand the performance change induced by doping in BFO. As a powerful technique for local structure determination of doping sites in substituted samples, X-ray absorption fine structure (XAFS) spectroscopy has been chosen in doped BFO researches due to its element selectivity and sensitivity to local structure around absorber [29–32], but most of the approaches only show the XAFS spectra of major elements Bi and/or Fe, and there is a lack of in-depth analysis on the doped ions. Therefore, further investigation on the local structure around doped-ion is still lacking, and it is necessary to explore the evolution of magnetic property in doped BFO especially focusing on the local structure.

In this work, BFO, $Bi_{0.9}La_{0.1}FeO_3$ (BLFO), and $BiFe_{0.9}Mn_{0.1}O_3$ (BFMO) powder samples were prepared by a gentle hydrothermal process, and the manifestations of structure and magnetic property driven by doping ions were studied systematically. The purpose is to provide further experimental and theoretical evidence to investigate the La/Mn doping effect in BFO. Therefore, the structure and morphologic and magnetic properties of all the as-prepared samples were characterized by X-ray diffraction (XRD), scanning electron microscope (SEM), and super-conducting quantum interference device (SQUID). In addition, the local structures around major elements Bi and Fe, as well as doping atoms La and Mn, were explored using XAFS spectroscopy, combing multiple scattering ab initio calculation.

2 Experiment

Analytical grade bismuth nitrate pentahydrate ($Bi(NO_3)_3{\cdot}5H_2O$), iron nitrate nonahydrate ($Fe(NO_3)_3{\cdot}9H_2O$), lanthanum nitrate hexahydrate ($La(NO_3)_3{\cdot}6H_2O$), and manganese nitrate hexahydrate ($Mn(NO_3)_3{\cdot}6H_2O$) were used as starting reagent. BFO, BLFO, and BFMO samples were prepared by conventional hydrothermal synthesis [29, 33]. Firstly, stoichiometric amounts of ($Bi(NO_3)_3{\cdot}5H_2O$), ($Fe(NO_3)_3{\cdot}9H_2O$), and ($La(NO_3)_3{\cdot}6H_2O$) or ($Mn(NO_3)_3{\cdot}6H_2O$) were respectively dissolved in distilled water under continuous stirring. After dissolving completely, Bi, Fe, and La or Mn solutions were mixed to form aqueous solutions. Then, the 4 M potassium hydroxide (KOH) solution was slowly added into the above solution under magnetic stirring to induce a co-precipitation reaction, obtaining a brown precipitate. Next, the as-prepared suspension solution was sealed in a 50-ml Teflon-lined autoclave for the hydrothermal reaction, which was heated up to 200 °C for 4 h. Finally, after cooling to room temperature naturally, the products were filtered, washed with distilled water, and dried at 60 °C for 2 h in an oven.

The crystalline structures of three resultant powders were determined by power XRD with D8 Advance X-ray diffractometer using Cu-Kα radiation (1.5406 Å). Scans were collected over an angular range of $15° \le 2\theta \le 79°$, with a step size of 0.02° (2θ). The morphologies of the samples were observed by the S-4800 SEM. Inductively coupled plasma mass spectrometry (ICP-MS) was used to analyze the true content of the doped elements in the samples. The Bi and La L_3-edge and Fe and Mn *K*-edge XAFS spectra of the as-prepared samples were measured at the 1W1B beamline of Beijing Synchrotron Radiation Facility (BSRF) in China in fluorescence mode using a Si (1 1 1) double-crystal monochromator at ambient condition. In this mode, an ionization chamber was used to detect the incident x-ray intensity, and the fluorescence intensity was monitored by a Lytle-type detector. The acquired XAFS raw data were background-subtracted, normalized, and Fourier transformed by the standard procedures with the IFEFFIT package [34]. The magnetic hysteresis loops of samples were measured using SQUID at room temperature.

A detailed X-ray absorption near edge structure (XANES) simulation was performed to help resolve the local structure around the selected elements (i.e., Bi, Fe, La, and Mn) in the samples, and the ab initio code FEFF9 within the real-space full multiple-scattering formalism [35] was performed to simulate the various possible locations for the doped La and Mn atoms in BFO. The clusters surrounding in the absorber La and Mn located at the crystallographically distinct sites were constructed in accordance with the crystal structure. All XANES spectra were calculated using the Hedin-Lundqvist self-energy together with the final state rule for the core–hole effect and full multiple scattering and convergence for self-consistency also have been achieved.

3 Results and Discussions

Powder XRD patterns of BFO, BLFO, and BFMO powders at room temperature are shown in Fig. 1. It can be seen that all samples are single phase without any impurity peaks. Furthermore, all diffraction peaks could be indexed as the pure BFO phase in a rhombohedrally distorted perovskite structure with a space group of *R*3*c* (JCPDS no. 71–2494). Besides, the diffraction peaks of BLFO and BFMO both have a slight relative shift to small angle compared with those of BFO, which may be mainly attributed to the fact that both the ionic radii of the doped elements La^{3+} (1.22 Å)

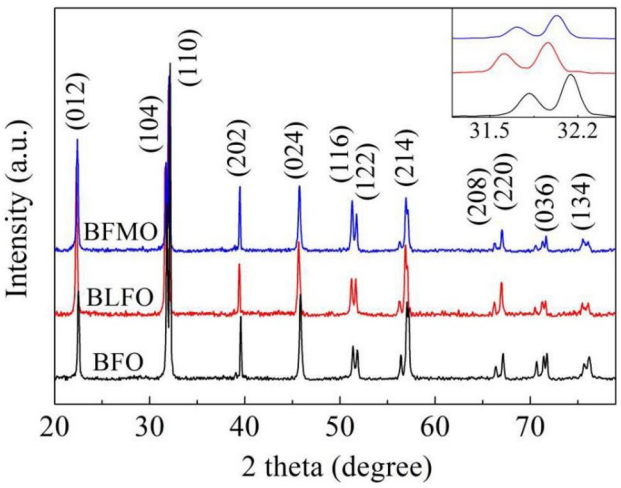

Fig. 1 XRD patterns of BFO, BLFO, and BFMO powders, inset: (104) and (110) peaks. Peaks are indexed according to hexagonal unit cell (JCPDS no.71–2494)

and Mn^{3+} (0.67 Å) are larger than those of Bi^{3+} (1.14 Å) and Fe^{3+} (0.64 Å). However, in most previous researches of doped BFO synthesized by various methods, such as solid-state reaction and sol–gel method, the structure transitions have already been observed at the same doping proportion [36–39], while the rhombohedral structure as pure BFO can be always maintained in the substituted samples prepared by the hydrothermal process [40–43].

In order to obtain the accurate concentrations of the substituted elements in two doped samples, the ICP-MS experiment has been done. Based on the results, the actual La content is only 0.893%, while the actual Mn content is only 0.786%, which are much less than the 10% doping content in the experiment, indicating that very few La and Mn atoms are able to enter BFO lattice during hydrothermal process. The low content, below 5% in BFO substitution, has been reported unable to induce the structure transition [44, 45]; therefore, the two doped samples in our experiment still maintain a single *R*3*c* symmetry. It can be observed that the content of La is higher than Mn, indicating that La atoms are easier to enter the BFO lattice. As a result, the larger difference in ion radius and the higher doping content make a greater lattice change in BLFO, which has been predicted by the greater shift of diffraction peak of BLFO in the inset of Fig. 1.

Figure 2 presents the morphological feature of all powder samples by using SEM technique, and the average particle sizes have been estimated from the standard log normal distribution functions shown in the histogram, respectively. As can be seen, though, these microstructures exhibit irregularly shaped particles, and the effect of doping with La/Mn in BFO can still be observed from the particle size. In Fig. 2a, the grain size of the irregular flakes is obviously uneven in BFO, which is about 90 nm. After doping elements, the average size of flakes changes to 50 nm for BLFO (Fig. 2b), while that of Mn-doped BFO turns to about 65 nm (Fig. 2c), respectively. Obviously, even in the case of low concentration, the particle dimensions can be affected by the substitution of La and Mn, and the particle size seems to be more sensitive to the larger ionic radius difference [32].

XAFS is a unique method that reflects the local structure of absorber by the shape and location of peaks, which are attributed to the complex multiple-scattering effect by the surrounding atoms. The Bi L_3-edge and Fe *K*-edge XANES spectra of BFO, BLFO, and BFMO are shown in Fig. 3. It can be observed that the Bi L_3-edge XANES spectra of doped samples show a similar profile as pure BFO in Fig. 3a, indicating that the local structure of Bi atoms is consistent, and the rhombohedral *R*3*c* phase is the dominator in both BLFO and BFMO as pure BFO. The approximately same shape and positions, which are close to those of Bi_2O_3 [46], imply the Bi^{3+} valence state in all samples without charge transfer from the Bi cations. Besides, the high intensity of two clear post-edge peaks in BLFO in inset Fig. 3a (labeled

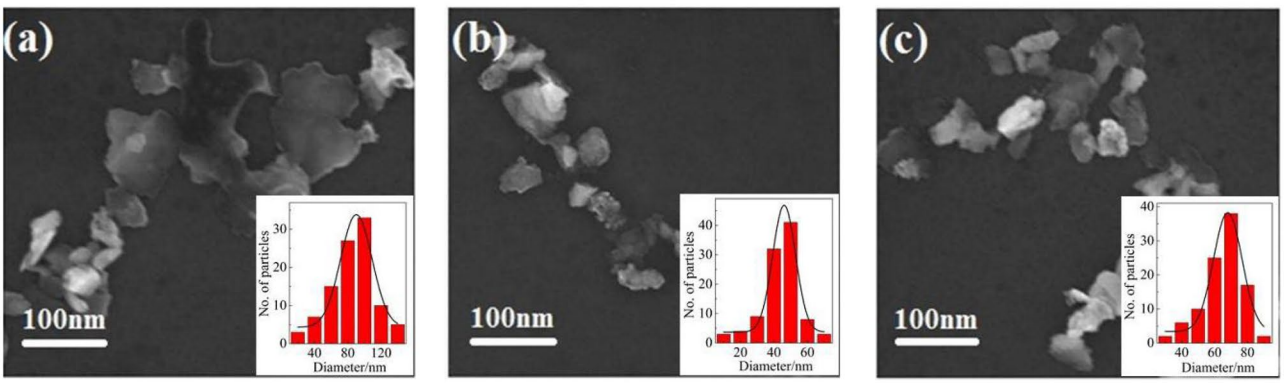

Fig. 2 SEM images of the powders of **a** BFO, **b** BLFO, **c** BFMO

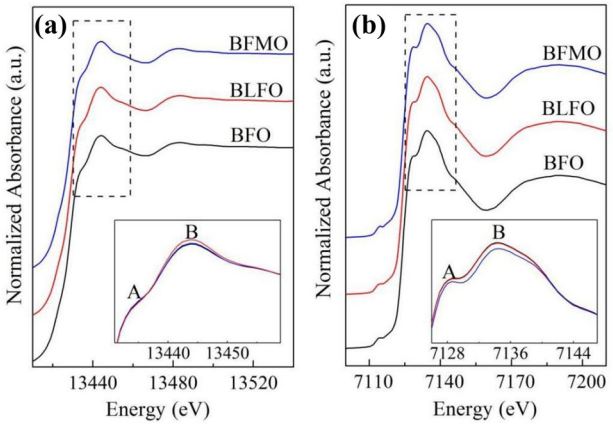

Fig. 3 **a** Normalized Bi L_3-edge and **b** Fe *K*-edge XANES spectra of BFO, BLFO, and BFMO

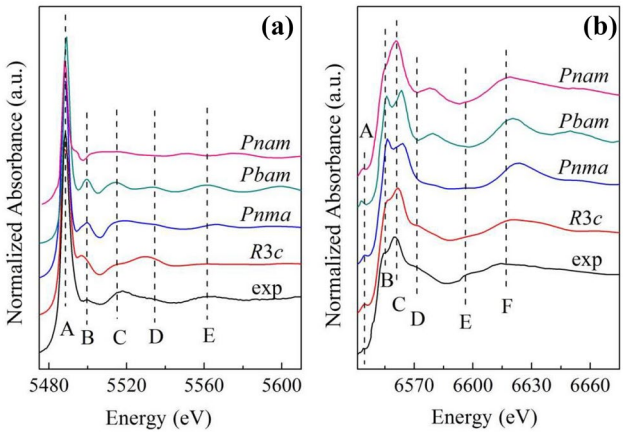

Fig. 4 **a** The measured La L_3-edge XANES spectrum of BLFO compared with the calculated XANES spectra with the substitution of La at the Bi site and **b** the measured Mn *K*-edge XANES spectrum of BFMO compared with the calculated XANES spectra with the substitution of Mn at the Fe site in different possible BFO structures where symmetries are *R*3*c*, *Pnma*, *Pbam*, and *Pnam*

A and B), which are caused by electron transition from Bi 2*p* to 6*d* state, explores that La doping has a great impact on the variations of the electronic structure of Bi^{3+} than Mn. Similar results are obtained from the Fe *K*-edge XANES spectra in Fig. 3b. The almost same profile without obvious energy shift for the absorption is consistent with that of Fe_2O_3 [47], suggesting that all samples keep the original rhombohedral *R*3*c* phase, and the oxidation state of Fe is corresponded to Fe^{3+}, instead of a transition to Fe^{2+}. While the shoulder peak A (inset Fig. 3b) is caused by the partial transfer of 2p electrons in oxygen 2p band to the Fe 3d orbital [48], peak B (inset Fig. 3b) represents the 1 dipole-allowed transition to an unoccupied 4p orbital [49], and the lower intensity of peaks A and B in BFMO, related to the charge transfer from the O 2p states to Fe 3d states and 3d-4p orbital hybridization, illustrates that Mn-doping has a stronger impact on Fe than La-doping. Therefore, low-concentration La/Mn substitution can only slightly affect the electronic structure of the main elements at their doping sites without any obvious effect on its parent structure.

Although the results of XANES spectra of the major elements Bi and Fe in pure and doped samples are consistent with the XRD conclusions, of great interest, the XAFS spectra of doping elements La and Mn are still measured to obtain a more direct insight into the local structural arrangement for the doped samples. The La L_3-edge XAFS spectrum of BLFO and the Mn *K*-edge XAFS spectra BFMO are shown in Fig. 4, and to gain the accurate information about the location of La and Mn atoms in the doped BFO lattice, we resort to the XANES simulation, which has been successfully applied to identify the phase structure for the absorbers [35, 50, 51]. The calculations are based on the most plausible structures for doped BFO samples that have been reported in the previous literature, and the model structures are constructed by the substitution of one doped atom at the Bi or Fe site, using the same parameter as our published reports [29, 32]. As shown in Fig. 4a, the calculated XANES spectra of La-substituted Bi based on *R*3*c*, *Pnma* [52], *Pbam* [53], and *Pnam* [54] symmetry are firstly constructed. Comparing the experimental data, the theoretical spectrum of *R*3*c* shows large discrepancy in the peak intensity ratios for the post-edge features of B, C, and D, indicating that the local environment of the doped La in BFO lattice has changed. For the *Pnam*, the experimental features A–D can be correctly reproduced, but the energy values of those peaks are not ideal. In contrast, it is surprising that an excellent agreement between the experimental and theoretical spectra is obtained for the *Pnma*, as well as the *Pbam* structural model, implying that the local structure around La ions has been induced to orthorhombic symmetry when La substituted Bi sites in BFO. We then calculate the Mn *K*-edge XANES spectra of the same structures as the calculation for BLFO, and the model structures are constructed by the substitution of Mn at the Fe site, as shown in Fig. 4b. Unlike La doping, the calculated spectrum based on the structure with *R*3*c* symmetry coincides with the experimental spectrum for BFMO, while the other symmetry structures are distinctly different, illustrating that Mn doping has no effect on its local structure although it is still a substitution for Fe in BFO lattice.

At this stage, a significant problem needs to be solved urgently concerning the existent form of the orthorhombic symmetry in BLFO: why is there no trace of the mixed phases detected in the XRD pattern of BLFO? Actually, all features of La L_3-edge and Mn *K*-edge XANES spectra are reproduced by using a cluster (radius of not less than 8.0 Å) with 185 atoms; as a result, it can be concluded that the

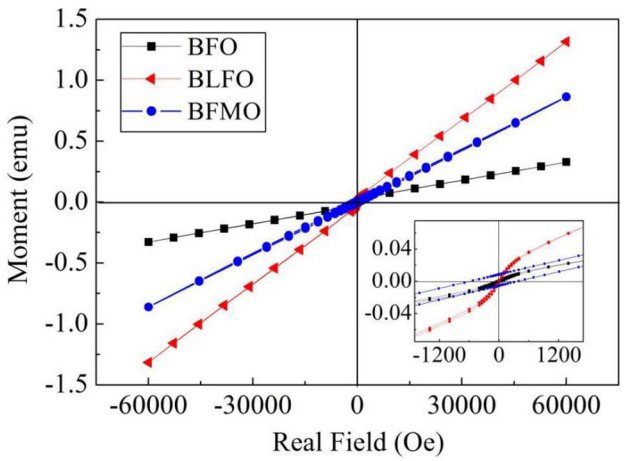

Fig. 5 Magnetic hysteresis loops of BFO, BLFO, and BFMO samples at room temperature

phase transition from *R*3*c* symmetry to orthorhombic is a nanoscale phase transition, so the size of the mixed phases may be too small to be examined by XRD. In addition, the small amount of these nanoparticles with orthorhombic symmetry due to the low actual doping concentration may be the other reason, which makes the mixed phases cannot be observed. Moreover, the forms of existence of nanoparticles with orthorhombic symmetry induced by La doping are various; they may exist alone, or may be embedded in a BFO matrix with *R*3*c* symmetry, or embedded on the surface of BFO particles, or the above situations may occur, making the detection of the mixed phases more difficult. Therefore, the divergence in the XANES spectra of doped La and Mn elements not only confirms that B-site doping seems to have a weaker influence on the stability than that of A-site doping, but also makes up for the limitations of our XRD result, as well as the results revealed by the XANES spectra of main elements in doped BFO samples.

The magnetic hysteresis loops of pure and doped BFO samples with applied magnetic field of 60 kOe at room temperature are depicted in Fig. 5. The magnetic hysteresis loop of BFO is nearly a straight line indicating the antiferromagnetic nature of pure BFO, and its weak magnetization implies the existence of nanoparticles that have been observed in SEM pattern; otherwise, magnetism will not be observed due to a cancellation of magnetization on macroscopic scale subjected by cycloidal modulation of 62 nm [55]. Though the strong magnetic interaction is expected between the high-spin state Fe^{3+} ions [56], stronger magnetism is obtained by doping La at Bi site in BFO because of the smaller particle size and higher doping concentration. Besides, the magnetic hysteresis loop of BLFO is no longer linear in inset Fig. 4, indicating the appearance of ferromagnetic property, while BFMO is obviously antiferromagnetic. The weak ferromagnetism observed in the doped BFO system is usually attributed to the canting of antiferromagnetically ordered spins by a distortion of the structure [57, 58]. Considering the results of XANES spectra of the doping elements La and Mn, we infer that the ferromagnetism of BLFO may be caused by the nanoparticles with orthorhombic symmetry, which may have changed the Fe–O–Fe angle and subsequently the magnetization [59]. Therefore, our results of about 1% of the actual concentration of La/Mn substituted at different sites in BFO lattices show that doping elements are possible to enhance magnetization, and the appearance of the nanoscale phase transition has influence on the magnetism for BFO system.

4 Conclusion

In summary, we prepared pure and doped BFO powders with 10% La/Mn dopant concentration by the hydrothermal method, and ICP-MS results show that only up to 1% La/Mn is actually doped into the BFO lattice. All samples show irregularly shaped particles, and the size of nanoparticles becomes uniform after doping. XRD results and XAFS results of the main elements Bi and Fe confirm that the structures are still *R*3*c* symmetric in all samples. However, our experimental and theoretical investigation on the doped La L_3-edge reveals the existence of secondary nanoparticles with orthorhombic symmetry, which might be responsible for its obvious ferromagnetism, while the local structure of Mn keeps the *R*3*c* symmetry, and BFMO is antiferromagnetic as the pure BFO, though doping La/Mn does enhance the magnetization of BFO. The special insight demonstrates that it is particularly important to identify the local structure for the phase classification, and it may provide a new perspective for exploring the underlying multiferroic mechanism in BFO-based materials.

Funding This work is supported by the Fundamental Research Funds for the Central Universities (grant no. ZY20210320).

Declarations

Competing Interests The author declares no competing interests.

References

1. Yuan, X.Y., Shi, L., Zhao, J.Y., Zhou, S.M., Li, Y., Xie, C.Z., Guo, J.H.: Sr and Pb co-doping effect on the crystal structure, dielectric and magnetic properties of $BiFeO_3$ multiferroic compounds. J. Alloy. Compd. **708**, 93–98 (2017). https://doi.org/10.1016/j.jallcom.2017.02.288

2. Rojac, T., Bencan, A., Malic, B., Tutuncu, G., Jones, J.L., Daniels, J.E., Damjanovic, D.: $BiFeO_3$ ceramics: processing, electrical, and electromechanical properties. J. Am. Ceram. Soc. **97**(7), 1993–2011 (2014). https://doi.org/10.1111/jace.12982
3. Vashisth, B.K., Bangruwa, J.S., Beniwal, A., Gairola, S.P., Kumar, A., Singh, N., Verma, V.: Modified ferroelectric/magnetic and leakage current density properties of Co and Sm co-doped bismuth ferrites. J. Alloy. Compd. **698**, 699–705 (2017). https://doi.org/10.1016/j.jallcom.2016.12.278
4. Singh, A., Pandey, V., Kotnala, R.K., Pandey, D.: Direct evidence for multiferroic magnetoelectric coupling in 09 $BiFeO_3$–0.1$BaTiO_3$. Phys. Rev. Lett. **101**, 247602 (2008). https://doi.org/10.1103/PhysRevLett.101.247602
5. Beniwal, A., Bangruwa, J.S., Walia, R.: Verma, V: A systematic study on multiferroics $Bi_{1-x}Ce_xFe_{1-y}Mn_yO_3$: structural, magnetic and electrical properties. Ceram. Int. **42**, 10373–10379 (2016). https://doi.org/10.1016/j.ceramint.2016.03.169
6. Anju, A., Agarwal, A., Agarwal, P., Aghamkar, V., Singh, O., Kumar, A.: Structural transitions and multiferrocity in Ba and Co substituted nanosized bismuth ferrite. J. Alloy. Compd. **697**, 333–340 (2017). https://doi.org/10.1016/j.jallcom.2016.12.082
7. Jarrier, R., Marti, X., Herrero-Albillos, J., Ferrer, P., Haumont, R., Gemeiner, P., Geneste, G., Berthet, P., Schülli, T., Cevc, P., Blinc, R., Wong, S.S., Park, T.J., Alexe, M., Carpenter, M.A., Scott, J.F., Catalan, G., Dkhil, B.: Surface phase transitions in $BiFeO_3$ below room temperature. Phys. Rev. B **85**(18), 184104 (2012). https://doi.org/10.1103/PhysRevB.85.184104
8. Arya, G., Kotnala, R.K., Negi, N.S.: A novel approach to improve properties of $BiFeO_3$ nanomultiferroics. J. Am. Ceram. Soc. **97**(5), 1475–1480 (2014). https://doi.org/10.1111/jace.12782
9. Vanga, P.R., Mangalaraja, R.V., Giridharan, N.V., Ashok, M.: Influence o divalent Ni and trivalent Cr ions on the properties of ytterbium modified bismuth ferrite. J. Alloy. Compd. **684**, 55–61 (2016). https://doi.org/10.1016/j.jallcom.2016.05.138
10. Yang, C.H., Kan, D., Takeuchi, I., Nagarajan, V., Seidel, J.: Doping $BiFeO_3$: approaches and enhanced functionality. Phys. Chem. Chem. Phys. **14**(46), 15953–15962 (2012). https://doi.org/10.1039/c2cp43082g
11. Kumar, P., Kar, M.: Tuning of net magnetic moment in $BiFeO_3$ multiferroics by co-substitution of Nd and Mn. Physica B **448**, 90–95 (2014). https://doi.org/10.1016/j.physb.2014.03.080
12. Sati, P.C., Kumar, M., Chhoker, S.: Low temperature ferromagntic ordering and dielectric properties of $Bi_{1-x}Dy_xFeO_3$ ceramics. Ceram. Int. **41**(2), 3227–3236 (2015). https://doi.org/10.1016/j.ceramint.2014.11.012
13. Kan, D., Pálová, L., Anbusathaiah, V., Cheng, C.J., Fujino, S., Nagarajan, V., Rabe, K.M., Takeuchi, I.: Universal behavior and electric-field-induced structural transition in rare-earth-substituted $BiFeO_3$. Adv. Funct. Mater. **20**(7), 1108–1115 (2010). https://doi.org/10.1002/adfm.200902017
14. Das, R., Sharma, S., Mandal, K.: Aliovalent Ba^{2+} doping: a way to reduce oxygen vacancy in multiferroic $BiFeO_3$. J. Magn. Magn. Mater. **401**, 129–137 (2016). https://doi.org/10.1016/j.jmmm.2015.10.022
15. Ramachandran, B., Dixit, A., Naik, R., Lawes, G., Rao, M.S.R.: Weak ferromagnetic ordering in Ca doped polycrystalline $BiFeO_3$. J. Appl. Phys. **111**, 023910 (2012). https://doi.org/10.1063/1.3678449
16. Karpinsky, D.V., Troyanchuk, I.O., Mantytskaya, O.S., Chobot, G.M., Sikolenko, V.V., Efifimov, V., Tovar, M.: Magnetic and piezoelectric properties of the Bi1-xLaxFeO3 system near the transition from the polar to antipolar phase. Phys. Solid State **56**, 701–706 (2014). https://doi.org/10.1134/S106378341404012X
17. Rangi, M., Sanghi, S., Jangra, S., Kaswan, K., Khasa, S., Agarwal, A.: Crystal structure transformation and improved dielectric and magnetic properties of La-substituted $BiFeO_3$ multiferroics. Ceram. Int. **43**, 12095–12101 (2017). https://doi.org/10.1016/j.ceramint.2017.06.065
18. Liu, K.T., Li, J., Xu, J.B., Xu, F.L., Wang, L., Bian, L.: Study on dielectric, optic and magnetic properties of manganese and nickel co-doped bismuth ferrite thin film. J. Mater. Sci: Mater. Electron. **28**, 5609–5614 (2017). https://doi.org/10.1007/s10854-016-6229-z
19. Ge, W.N., Rahman, A., Cheng, H.R., Zhang, M., Liu, J.D., Zhang, Z.M., Ye, B.J.: Probing the role of cation vacancies on the ferromagnetism of La-doped $BiFeO_3$ ceramics. J. Magn. Magn. Mater. **449**, 401–405 (2018). https://doi.org/10.1016/j.jmmm.2017.10.082
20. Masoudpanah, S.M., Mirkazemi, S.M., Bagheriyeh, R., Jabbari, F., Bayat, F.: Structural, magnetic and photocatalytic characterization of Bi1-xLaxFeO3 nanoparticles synthesized by thermal decomposition method. Bull. Mater. Sci. **40**, 93–100 (2017). https://doi.org/10.1007/s12034-016-1346-0
21. Wang, K.F., Liu, J.M., Ren, Z.F.: Multiferroicity: the coupling between magnetic and polarization orders. Adv. Phys. **58**, 321–448 (2009). https://doi.org/10.1080/00018730902920554
22 Yan, F.X., Han, K., Jiao, Z.C., Zhao, G.Y., Wang, T., Guo, M.L., Chen, Y.Q.: Crating-patterned $Bi_{0.85}La_{0.15}Fe_{0.95}Mn_{0.05}O_3$ epitaxial thin film prepared using photosensitive sol-gel method and its ferromagnetic and ferroelectric properties. J. Alloy. Compd. **728**, 152–158 (2017). https://doi.org/10.1016/j.jallcom.2017.08.283
23. Han, Y.M., Ma, Y.H., Quan, C.Y., Gao, N., Zhang, Q.X., Mao, W.W., Zhang, J., Yang, J.P., Li, X.A., Huang, W.: Substitution-driven structural, optical and magnetic transformation of Mn, Zn doped $BiFeO_3$. Ceram. Int. **41**(2), 2476–2483 (2015). https://doi.org/10.1016/j.ceramint.2014.10.065
24. Kader, S.M.A., Ruth, D.E.J., Babu, M.V.G., Muneeswaran, M., Giridharan, N.V., Sundarakannan, B.: Investigations on the effect of Ba and Zr co-doping on the structural, thermal, electrical and magnetic properties of $BiFeO_3$ multiferroics. Ceram. Int. **43**(17), 15544–15550 (2017). https://doi.org/10.1016/j.ceramint.2017.08.104
25 Baun, I.B.S., Lakshmi, S.D.: Simultaneous enhancement of room temperature multiferroic properties of $BiFeO_3$ by Nd doping at Bi site and Co doping at Fe site. J. Mater. Sci.: Mater. Electron. **28**, 16044–16052 (2017). https://doi.org/10.1007/s10854-017-7504-3
26. Chandel, S., Thakur, P., Tomar, M., Gupta, V., Thakur, A.: Investigation of structural, optical, dielectric and magnetic studies of Mn substituted $BiFeO_3$ multiferroics. Ceram. Int. **43**(16), 13750–13758 (2017). https://doi.org/10.1016/j.ceramint.2017.07.088
27 Pradhan, D.K., Choudhary, R.N.P., Rinaldi, C., Katiyar, R.S.: Effect of Mn substitution on electrical and magnetic properties of $Bi_{0.9}La_{0.1}FeO_3$. J. Appl. Phys. **106**, 024102 (2009). https://doi.org/10.1063/1.3158121
28. Dhanalakshmi, B., Pratap, K., Rao, B.P., Rao, P.S.V.S.: Effects of Mn doping on structural, dielectric and multiferroic properties of $BiFeO_3$ nanoceramics. J. Alloy. Comp. **676**, 193–201 (2016). https://doi.org/10.1016/j.jallcom.2016.03.208
29. Wang, Y.: Pressure induced phase transition of La-substituted $BiFeO_3$. Solid State Commun. **341**, 114595 (2022). https://doi.org/10.1016/j.ssc.2021.114595
30. Gholam, T., Ablat, A., Mamat, M., Wu, R., Aimidula, A., Bake, M.A., Zheng, L., Wang, J., Qian, H., Wu, R.: Local electronic structure analysis of Zn-doped $BiFeO_3$ powders by X-ray absorption fine structure spectroscopy. J. Alloy. Comp. **710**, 843–849 (2017). https://doi.org/10.1016/j.jallcom.2017.03.242
31. Gholam, T., Ablat, A., Mamat, M., Wu, R., Aimidula, A., Bake, M.A., Zheng, L.R., Wang, J.O., Qian, H.J., Wu, R., Ibrahim, K.: An experimental study of the local electronic structure of B-site gallium doped bismuth ferrite powders. Phys. Lett. A **381**(29), 2367–2373 (2017). https://doi.org/10.1016/j.physleta.2017.05.007

32. Wang, Y., Guo, Z.Y., Jia, Q.J., Dong, J.C., Zhang, J., Chen, D.L.: Effect of Nd/Mn substitution on the structure and magnetic properties of nano-$BiFeO_3$. J. Alloys Compd. **786**, 385–393 (2019). https://doi.org/10.1016/j.jallcom.2019.01.369
33. Du, Y., Cheng, Z.X., Shahbazi, M., Collings, E.W., Dou, S.X., Wang, X.L.: Enhancement of ferromagnetic and dielectric properties in lanthanum doped $BiFeO_3$ by hydrothermal synthesis. J. Alloys Compd. **490**(1–2), 637–341 (2010). https://doi.org/10.1016/j.jallcom.2009.10.124
34. Ravel, B., Newville, M.: ATHENE, ARTEMIS, HEPHAESTUS: data analysis for X-ray absorption spectroscopy using IFEFFIT. J. Synchrotron Rad. **12**, 537–541 (2005). https://doi.org/10.1107/S0909049505012719
35. Rehr, J.J., Albers, R.C.: Theoretical approaches to x-ray absorption fine structure. Rev. Mod. Phys. **72**, 621 (2000). https://doi.org/10.1103/RevModPhys.72.621
36. Kumar, A., Varshney, D.: Crystal structure refinement of $Bi_{1-x}Nd_xFeO_3$ multiferroic by the Rietveld method. Ceram. Int. **38**(5), 3935–3942 (2012). https://doi.org/10.1016/j.ceramint.2012.01.046
37. Liu, S., Luo, H., Yan, S.Q., Yao, L.L., He, J., Li, Y.H., He, L.H., Huang, S.X., Deng, L.W.: Effect of Nd-doping on structure and microwave eletromagnetic properties of $BiFeO_3$. J. Magn. Magn. Mater. **426**, 267–272 (2017). https://doi.org/10.1016/j.jmmm.2016.11.080
38 Yuan, G.L., Or, S.W., Chan, H.L.W.: Structure transformation and ferroelectric-paraelectric phase transition in $Bi_{1-x}La_xFeO_3$ (x= 0–0.25) mulfiferroic ceramics. J. Phys. D: Appl. Phys. **40**, 1196 (2007). https://doi.org/10.1088/0022-3727/40/4/043
39. Pandit, P., Satapathy, S., Gupta, P.K.: Effect of La substitution on conductivity and dielectric properties of $Bi_{1-x}La_xFeO_3$ ceramics: an impedance spectroscopy analysis. Physica B **406**(13), 2669–2677 (2011). https://doi.org/10.1016/j.physb.2011.03.081
40. Basu, S., Hossain, S.K.M., Chakravorty, D., Pal, M.: Enhanced magnetic properties in hydrothermally synthesized Mn-doped $BiFeO_3$ nanoparticles. Curr. Appl. Phys. **11**(4), 976–980 (2011). https://doi.org/10.1016/j.cap.2010.12.034
41. Pei, Y.L., Zhang, C.L.: Effect of ion doping in different sites on morphology and photocatalytic activity of $BiFeO_3$ microcrystals. J. Alloy. Compd. **570**, 57–60 (2013). https://doi.org/10.1016/j.jallcom.2013.03.176
42. Chen, Z.W., Li, Y.F., Wu, Y.P., Hu, J.Q.: Hydrothermal synthesis and mechanism and property study of La-doped $BiFeO_3$ crytallites. J. Mater. Sci. Mater. Electron. **23**, 1402–1408 (2012). https://doi.org/10.1007/s10854-011-0605-5
43. Du, Y., Cheng, Z.X., Dou, S.X., Shahbazi, M., Wang, X.L.: Enhancement of magnetization and dielectric properties of chromium-doped $BiFeO_3$ with tunable morphologies. Thin Solid Films **518**(24), e5–e8 (2010). https://doi.org/10.1016/j.tsf.2010.03.118
44. Tang, P., Kuang, D.H., Yang, S.H., Zhang, Y.L.: Hydrothermal synthesis and structural, morphologic and magnetic characteristics of Mn doped bismuth ferrite crystallites. J. Mater. Sci. Mater. Electron. **27**, 2594–2600 (2016). https://doi.org/10.1007/s10854-015-4063-3
45. Tlemcani, T.S., Bahraoui, T.E., Taibi, M., Belayachi, A., Schmerbe, G., Dinia, A., Lefdil, M.A.: Effect of Nd substitution on physical properties of multiferroic compound $BiFeO_3$. J. Sol. Gel Sci. Technol. **73**, 637–678 (2015). https://doi.org/10.1007/s10971-015-3654-z
46. Ankudinov, A.L., Bouldin, C.E., Rehr, J.J., Sims, J., Hung, H.: Parallel calculation of electron multiple scattering using Lanczos algorithms. Phys. Rev. B **65**, 104107 (2002). https://doi.org/10.1103/PhysRevB.65.104107
47. Ankudinov, A.L., Ravel, B., Rher, J.J., Conradson, S.D.: Real-space multiple-scattering calculation and interpretation of x-ray-absorption near-edge structure. Phys. Rev. B **58**, 7565 (1998). https://doi.org/10.1103/PhysRevB.58.7565
48 Yotburut, B., Yamwong, T., Thongbai, P., Maensiri, S.: Synthesis and characterization of coprecipitation-prepared La-doped $BiFeO_3$ nanopowders and their bulk dielectric properties. Jpn. J. Appl. Phys. **53**, 06GJ13 (2014). https://doi.org/10.7567/jjap.53.06jg13
49. Lee, D.G., Kim, M.G., Ryu, S., Jang, H.M., Lee, S.G.: Epitaxially grown La-modified $BiFeO_3$ magnetoferroelectric thin films. Appl. Phys. Lett. **86**, 222903 (2005). https://doi.org/10.1063/1.1941474
50. Ishimatsu, N., Watanabe, T., Oka, K., Azuma, M., Mizumaki, M., Nitta, K., Ina, T., Kawamura, N.: Differences in local structure around Co and Fe of the $BiCo_{1-x}Fe_xO_3$ system determined by x-ray absorption fine structure. Phys. Rev. B **92**, 054108 (2015). https://doi.org/10.1103/PhysRevB.92.054108
51 Jutimoosik, J., Hunpratub, S., Maensiri, S., Rujirawat, S., Yimnirun, R.: On preferred Mn site in multiferroic $BiFeO_3$: a view by synchrotron x-ray absorption near edge structure spectroscopy. J. Appl. Phys. **116**, 104105 (2014). https://doi.org/10.1063/1.4895474
52. Vázquez, O.E.G., Wojdeł, J.C., Diéguez, O., Íñiguez, J.: First-principles investigation of the structural phases and enhanced response properties of the $BiFeO_3$-$LaFeO_3$ multiferroic solid solution. Phys. Rev. B **85**, 064119 (2012). https://doi.org/10.1103/PhysRevB.85.064119
53. Troyanchuk, I.O., Karpinsky, D.V., Bushinsky, M.V., Khomchenko, V.A., Kakazei, G.N., Araujo, J.P., Tovar, M., Sikolenko, V., Efimov, V., Kholkin, A.L.: Isothermal structural transitions, magnetization and large piezoelectric response in $Bi_{1-x}La_xFeO_3$ perovskites. Phys. Rev. B **83**, 054109 (2011). https://doi.org/10.1103/PhysRevB.83.054109
54. Yu, C.Y., Viola, G., Zhang, D., Zhou, K.C., Koval, B., Mahajan, A., Wilson, R.M., Tarakina, N.V., Abrahams, I., Yan, H.X.: Phase evolution and electrical behaviour of samarium-substituted bismuth ferrite ceramics. J. Eur. Ceram. Soc. **38**(4), 1374–1380 (2018). https://doi.org/10.1016/j.jeurceramsoc.2017.12.016
55. Mazumder, R., Devi, P.S., Bhattacharya, D., Choudhury, P., Sen, A., Raja, M.: Ferromagnetism in nanoscale $BiFeO_3$. Appl. Phys. Lett. **91**, 062510 (2007). https://doi.org/10.1063/1.2768201
56. Goodenough, J.B.: Theory of the role of covalence in the perovskite-type manganites [La, M(II)] MnO_3. Phys. Rev. **100**, 564–573 (1955). https://doi.org/10.1103/physrev.100.564
57. Pradhan, S.K., Roul, B.K., Sahu, D.R.: Enhancement of ferromagnetism and multiferroicity in Ho doped Fe rich $BiFeO_3$. Solid State Commun. **152**(13), 1176–1180 (2012). https://doi.org/10.1016/j.ssc.2012.03.034
58. Moriya, T.: Anisotropic superexchange interaction and weak ferromagnetism. Phys. Rev. **120**, 91–98 (1960). https://doi.org/10.1103/PhysRev.120.91
59. Lü, F.C., Yin, K., Fu, K.X., Wang, Y.N., Ren, J., Xie, Q.: Enhanced magnetic and dielectric properties of Y doped bismuth ferrite nanofiber. Ceram. Int. **43**, 16101–16106 (2017). https://doi.org/10.1016/j.ceramint.2017.08.171